Mamatha K. M.

Department of Mechanical Engineering
Siddaganga Institute of Technology
Tumakuru 572103, Karnataka
India

U.S. Mallik

Department of Mechanical Engineering,
Siddaganga Institute of Technology
Tumakuru 572103, Karnataka
India

Vishwanath Koti

Department of Mechanical Engineering
Ramaiah Institute of Technology
Bengaluru 560054, Karnataka
India

K.V. Shivananda Murthy

Department of Mechanical Engineering
Government Sri Krishnarajendra Silver
Jubilee Technological Institute
Bengaluru 560001, Karnataka
India

Praveennath G. Koppad

Department of Mechanical Engineering
National Institute of Technology Karnataka
Mangalore 575025, Karnataka
India

Effect of Variations in Mn Content on Mechanical and Corrosion Characteristics of Cu-Al-Mn Shape Memory Alloys

In this work, the role of Mn on the shape memory effect and mechanical and corrosion behavior of Cu-Al-Mn shape memory alloys was studied. The composition of Al was fixed to 10 wt% while that of Mn was varied from 2 to 10 wt%. The strain recovery by SME was evaluated using the bend test, while the yield and ultimate tensile strength were obtained using the tension test. The corrosion behavior was studied using three different solutions: freshwater, substitute ocean water, and Hank's solution. The yield and ultimate tensile strength of Cu-Al-Mn alloys increased with Mn content up to 6%, which was attributed to grain refinement and precipitation hardening, while the fracture analysis showed mixed mode failure for all alloys. The corrosion behavior of Cu-Al-Mn alloys was modified due to the addition of Mn. With the increase in Mn content, the alloys displayed better corrosion resistance and lower corrosion rates. The corroded surface analysis tested in freshwater showed pitting corrosion, while Cu-Al-Mn alloy with low Mn content was tested in substitute ocean water. Hank's solution showed surface damage with an unstable surface layer.

***Keywords:** CuAlMn alloy; Shape memory alloys; Mechanical properties; Corrosion.*

1. INTRODUCTION

The material that exhibited the shape memory effect (SME) was first reported in the year 1951, and since then, a lot of alloy systems based on Au, Ni, Cu, Ti, and Fe have been developed [1-3]. The ability of alloy systems to regain their original shape after the appli–cation of thermal load has generated huge interest am–ong scientists and industrialists. This is because conventional materials are incapable of responding to the changes taking place in the surrounding environ–ment and are unable to operate in such service conditions. Shape memory alloys (SMA), which they are popularly known as can adapt and operate in such diverse operating conditions. The functional properties of SMA and its applications are related to temperature and stress-induced phase transitions. These materials are used in the development of smart devices, which in turn are used in the structures to conduct different functions such as monitoring, sensing, self-adapting, and actua–tion of structures. Since SMAs are stimuli-response materials, they are generally preferred in medicine, marine, aerospace, electrical, and structural engineering applications [4-7]. According to a survey reported in [8], the global SMA market was $11 billion in the year 2021 and is expected to reach $18.8 billion by 2026. In this regard, it is necessary to focus more research on the development of novel SMAs that can meet growing industrial demands.

There are many alloy systems, but only Cu- and Ni-based SMA alloys are commonly used because of their cost and properties. The Cu-based SMA systems are known for their flexibility in optimizing properties by tailoring their composition, allowing ease of fabrication, and widening the range of martensitic transformations. With or without other additions, alloys such as Cu-Al, Cu-Sn, and Cu-Zn have demonstrated good shape reco–very [9]. However, many of these alloys suffer from shortcomings such as brittleness, low strength, and poor thermal stability. Based on the composition and alloying additions these shortcomings are the result of large grain size and segregation of secondary phases at grain boun–daries. For instance, Cu-Al alloy is not considered for practical applications due to its high transformation temperature and high Al content with β_2 ordered struc–ture, making it too brittle. The mechanical properties and transformation temperatures are extremely sensitive to the composition and ternary element addition to bi–nary Cu alloys. Ternary addition of Mn, Zn, and Ni to the Cu-Al alloy is proven beneficial as these elements stabilize the β phase and improve the shape memory properties [10]. On the other hand, the increase in Al content has resulted in a decrease in the martensitic transformation temperatures [11]. Raju and Sampath [12] studied the effect of the ternary addition of Fe to Cu-Al alloy developed using induction melting. The variations in the Fe content had a significant influence on the transformation temperature and the formation of β_1' martensite was the main reason for it. The strain recovery in SME was found to be dependent on the

amount of martensite phase present in the alloys. Pinto et al. [13] studied the effect of different ternary additions of Be, Mn, and Ag on the microhardness and electrical resistivity of Cu79Al19X2 alloys. The addition of Be decreased the microhardness of the Cu-rich solid solution, while Ag addition enhanced it considerably, and Mn addition had minimal influence. On a similar note, the electrical resistivity of the alloys decreased with Be and Ag addition while Mn addition had no significant influence. Moskvichev et al. [14] studied the microstructure and hardness of Cu-11Al-4Mn and Cu-11Al-9Mn alloys developed using electron beam melting with different heat inputs. The samples printed with high heat input showed eutectoid decomposition and formation of large grains of ordered β_1 phase. The hardness profile measured across different heights showed a sharp and smooth increase in the values in the transition zones. However, the addition of different Mn content to the Cu-Al alloy had no significant influence.

It is well known Cu alloys possess excellent corrosion resistance against unpolluted air, normal water, and marine environments. Specifically, in the case of Cu-Al alloys, the formation of protective films of Al_2O_3 and Cu_2O is considered the main reason for corrosion resistance [15,16]. However, the corrosion behavior of Cu-based SMAs has not been widely studied compared to other properties, such as damping performance. Most corrosion studies were performed on Cu-Al-Ni, Cu-Al-Be, and Cu-Zn-Al alloys in H_2SO_4 and NaCl environments. Montecinos and Simison [17] studied the effect of different Be content on the corrosion behavior of Cu-Al-Be alloy. According to anodic polarization curves, the Be content had no observable effect on the corrosion behavior, and corrosion pits were formed due to severe dealuminization. Based on chronoamperometric tests it was found that samples with single β phase were less susceptible to pit formation than the samples with precipitates. The influence of thermal treatment on the corrosion behavior of Cu-Al-Ni alloy was studied by Vrsalovic et al. [18] in 0.9%NaCl solution. The heat-treated samples showed enhanced surface layer resistance and charge transfer resistance, indicating high corrosion resistance. The corroded surface analysis showed the formation of spikes of corrosion products and pits underneath the spikes indicating the occurrence of pitting corrosion in these alloys. A similar observation on Cu-Al-Mn alloy was reported by the same authors, who found enhanced corrosion resistance due to heat treatment [19]. The observation was made based on low corrosion current density and high polarization resistance values. The enhanced corrosion resistance was due to the formation of Mn oxide film and heat-treated alloy containing martensite microstructure only. Overall, the corrosion behavior of Cu-based SMAs in different corrosion media has not yet been studied.

In this paper, the main objective is to study the influence of varying Mn content on the mechanical and corrosion behavior of Cu-Al-Mn alloy systems. Most of the studies focussed on damping performance for vibration and noise reduction applications and hardly focused on mechanical properties, which are one of the main requirements of SMAs. The corrosion behavior of Cu-Al-Mn SMA's in different corrosion media is also the least explored domain. In this regard, an attempt is made to address these concerns by subjecting SMAs to tension tests and corrosion tests in fresh water, substitute ocean water, and Hank's solution.
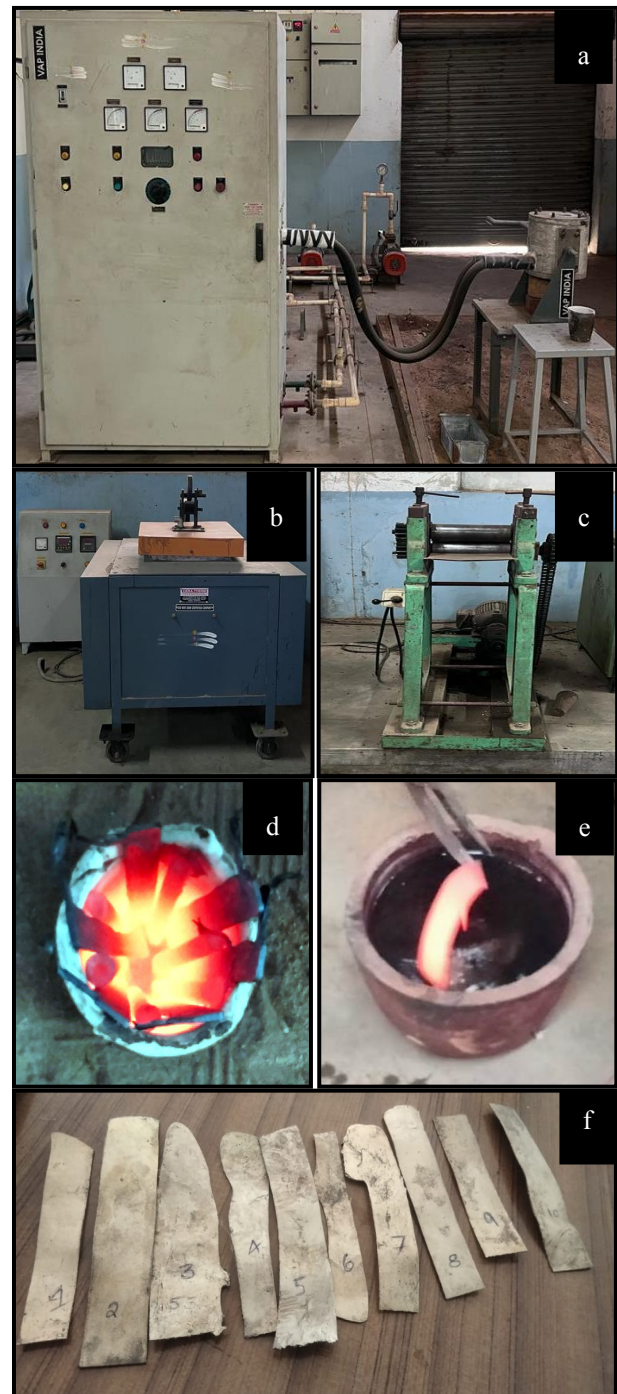

Figure 1. Photographs of (a) induction furnace, (ii) resistance furnace, (iii) rolling mill, (iv) heat treatment, (e) quenching, and (f) rolled Cu-Al-Mn SMA's.

2. EXPERIMENTAL DETAILS

2.1 Alloy preparation

High-purity Cu, Al, and Mn were selected as the starting materials to develop copper-based shape me–mory alloys, which were procured from Fenfe Metal–lurgical, India. The Cu-Al-Mn SMA's with different combinations of these three metals were prepared using the casting pro–

cess. The predefined chemical compo–sition of the alloys to be prepared is presented in Table 1. For making different samples appropriate metals are weighed and placed in an induction furnace (Make: VAP Induction Pvt. Ltd., India) for melting. After the melting process, the molten metal was poured into a mold made up of cast iron (120×100×3, mm^3) and allo–wed to solidify in the mold itself. All samples were homogenized at 900°C for about 1 h using a resistance furnace (Make: Cera-Therm International, India). In the next step, the samples were hot rolled using a rolling mill to obtain a thickness of 1 mm. Here, the final thic–kness was obtained after the samples were subjected to multi-pass rolling and inter–mittent annealing at 900°C for about 5 min. Followed by hot rolling, the samples were betatized at 900°C for about 3 h and then subjected to a two-step quenching process. In the first step, the samples were quenched in the boiling water maintained at 100°C for 5 min, and in the next step, they were quenched in the water maintained at room temperature. The step quenching process is adopted to avoid quenching cracks and overcome the brittleness of samples. The digital photographs of equipment used for fabri–cation, heat treatment, rolling mill, and hot rolled Cu-Al-Mn SMA's are presented in Fig. 1.

Table 1. Nomenclature and alloy compositions

Sample ID	Composition (Wt.%)		
	Cu	Al	Mn
C1	88	10	2
C2	86	10	4
C3	84	10	6
C4	80	10	10

Table 2 Preparation of solutions representative of substitute of ocean water

Stock solution No. 1		Stock solution No. 2		Stock solution No. 3	
Salts	Qty (g/L)	Salts	Qty (g/L)	Salts	Qty (g)
$MgCl_2 \cdot 6H_2O$	555.6	KCl	69.5	$Ba(NO_3)_2$	0.994
$CaCl_2$	57.9	$NaHCO_3$	20.1	$Mn(NO_3)_2 \cdot 6H_2O$	0.546
$SrCl_2 \cdot 6H_2O$	2.1	KBr	10.0	$Cu(NO_3)_2 \cdot 3H_2O$	0.396
		H_3BO_3	2.7	$Zn(NO_3)_2 \cdot 6H_2O$	0.151
		NaF	0.3	$Pb(NO_3)_2$	0.066
				$AgNO_3$	0.0049

2.2 Testing and characterization

The bend test on samples was conducted to determine the strain recovery by SME. For this, samples with 1 mm thickness obtained by hot rolling were used and subjected to bending. The bend angles just before and after heating were noted and substituted in the following equation to obtain strain recovery by SME [20].

$$SME\,(\%) = \theta_m / (180° - \theta_e)$$

where 'θ_m' and 'θ_e' are the angles recovered after unlo–ading and heating, respectively. Tensile properties of Cu-Al-Mn alloys were measured by conducting tests on the universal testing machine (Make: FIE Pvt. Ltd., India) with a deformation speed of 1 mm/min.

The corrosion behavior of Cu-Al-Mn SMA's in three different test solutions, fresh water, substitute oce–an water, and Hanks solution, was conducted. Before corrosion tests, the samples having the size of 20×20×1

mm^3 were finely polished using emery papers, followed by polycrystalline diamond polishing as an intermediate step and final polishing using polycrystalline alumina. The substitute ocean water was prepared as per ASTM D 1141-98 and the proportions of solutions required for preparation are presented in Table 2.

Table 3 Composition of Hank's solutions

Salt	Quantity (g/L)
NaCl	20
KCl	3
$NaHCO_3$	0.875
$CaCl_2$	0.35
$Na_2HPO_4 \cdot 2H_2O$	0.15
$MgCl_2 \cdot 6H_2O$	0.25
$MgSO_4 \cdot 7H_2O$	0.15
KH_2PO_4	0.15
Glucose	2.5

A detailed procedure for preparing substitute ocean water is provided in the aforementioned standard, but a brief description is provided here. In the first step, stock solution 1 is prepared by dissolving the calculated amount of salts in water and diluting it to a total volume of 7.0 L. In the second step, stock solution 2 is prepared by dissolving the salts in water, followed by diluting it to a total volume of 7.0 L. The preparation of stock solution 3 is almost the same as previous solutions except it is diluted to a total volume of 10.0 L. In the final step, to prepare 10.0 L of substitute ocean water, about 40.94 g of anhydrous Na_2SO_4 and 245.34 g of NaCl are added to 8 to 9.0 L of water. To this solution, about 200 mL of stock solution 1 is added slowly and stirred properly, followed by the addition of 100 mL of stock solution 2. Finally, about 10 mL of stock solution 3 is slowly added to this solution and stirred vigorously. The last corrosion media used was Hank's solution, which had pH and temperature maintained at 7.2 and 310 K. The composition of Hank's used for this work is presented in Table 3. The corrosion behavior of Cu-Al-Mn alloys was evaluated by electro–chemical measurement, which was conducted in a glass cell having a three-electrode assembly. The saturated calomel electrode (SCE) was the reference electrode, the graphite rod was the counter electrode, and the alloy sample was the working electrode. Here, the test solu–tions were freshwater, substitute ocean water, and Hanks solution. Before conducting electrochemical measu–rements the working electrode was kept in different test solutions for about 1 h to arrive at steady state open cir–cuit potential. The potentiodynamic polarization curves were obtained by employing a scan rate of 5 mVs^{-1} using potentiostat. The fracture surface post-tensile and corrosion tests were observed using a scanning electron microscope (Make: Tescan Vega3, India).

3. RESULTS AND DISCUSSION

The main concern in the development of Cu-Al-Mn SMA's was to maintain their composition during the casting process. This is quite essential to obtain a satis–factory degree of shape memory properties, and in order to analyze the composition, the quantitative EDAX analysis was conducted on all samples. Fig. 2 shows the EDAX pattern of Cu-Al-Mn SMA's, which confirms

the presence of all three major elements: Cu, Al, and Mn. Further, Fig. 3 shows the Al and Mn content in all alloys obtained from EDAX analysis. There is the pos–sibility that the Mn content might be reduced due to thermomechanical treatment. However, as seen in the figure, there is no change in the Al or Mn content, and it is almost the same as that mentioned in Table 1.
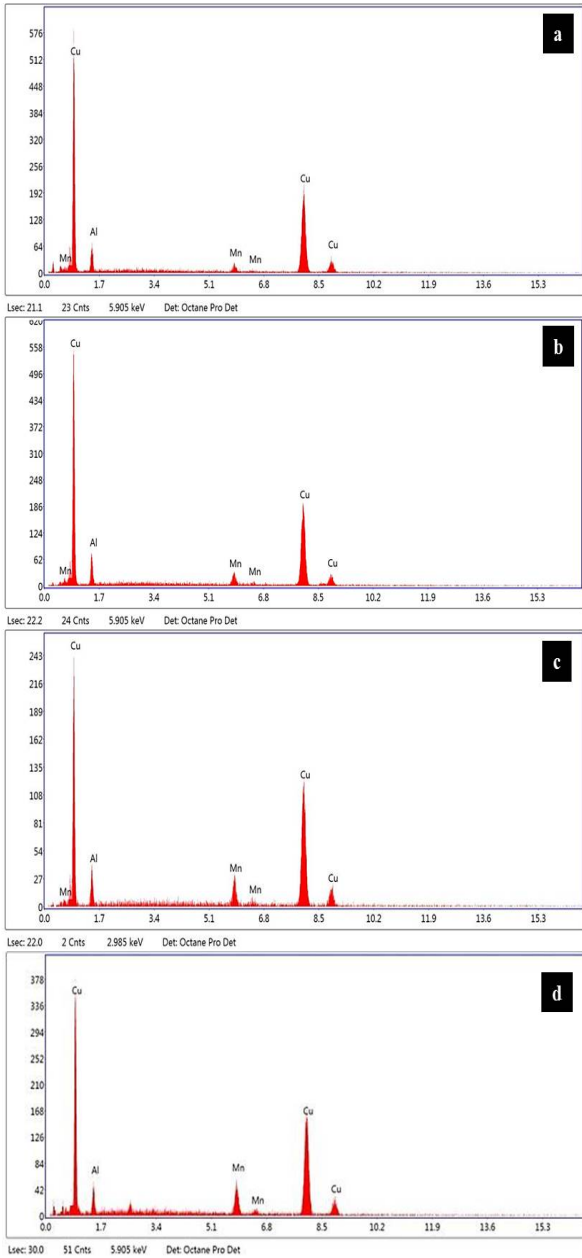

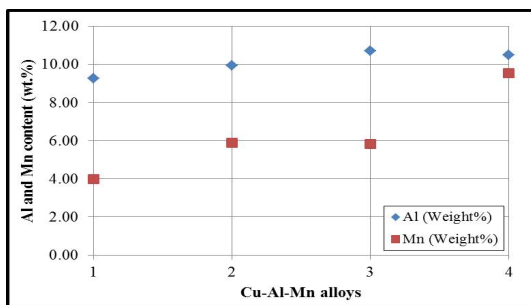Figure 2. EDAX analysis of (a) C1, (b) C2, (c) C3 and (d) C4.

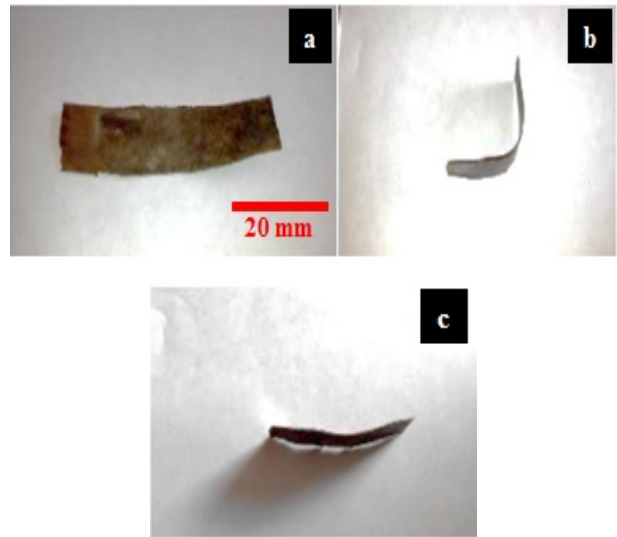Figure 3. Al and Mn content in Cu-Al-Mn SMAs was measured using EDAX.

Figure 4. Photograph showing C1 alloy prior to bending, after bending, and shape recovery post-heat treatment.

3.1 Shape memory effect

As mentioned in the experimental section, the bend test was conducted to obtain strain recovery by SME of all Cu-Al-Mn SMA's. The hot-rolled SMA samples having 1 mm thickness in their martensitic phase were bent to a U-shape at a temperature lower than the martensite finish temperature (M_f). After being subjected to bending at room temperature the Cu-Al-Mn SMA's were heated to a temperature above their austenite finish temperature (A_f). Fig. 4 shows the photograph of rolled sheets of C1 alloy prior to bending, deformed alloy post-bending, and shape recovery after heating. The angles after bending, that is, just before heating in the martensite phase, and after heating, which is the austenite phase of alloys, were recorded. Using these angles, the strain recovery by SME was calculated, and the values obtained are presented in Table 4. All the alloy systems showed significant strain recovery by SMEs ranging from 91-100%. As observed from the values, the strain recovery by SME tends to increase with the Mn content up to 6 wt% but decreases thereafter. The highest strain recovery by SME of 100% was displayed by C3 alloy, which indicates excellent thermomechanical stability, and this alloy has a higher proportion of martensite when compared to C1 or C4 alloys. This indicates that the addition of Mn was capable of enhancing the strain recovery by SME by precipitation hardening in the parent phase. The precipitates, along with the dislocation induced by deformation, stabilize the martensite [21,22].
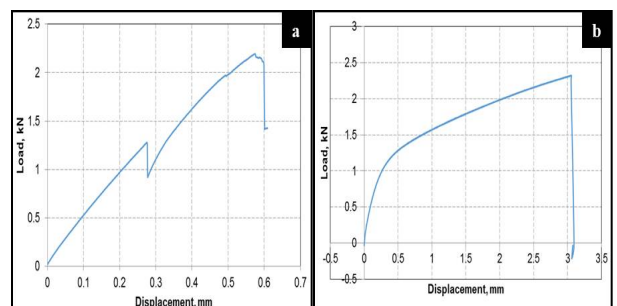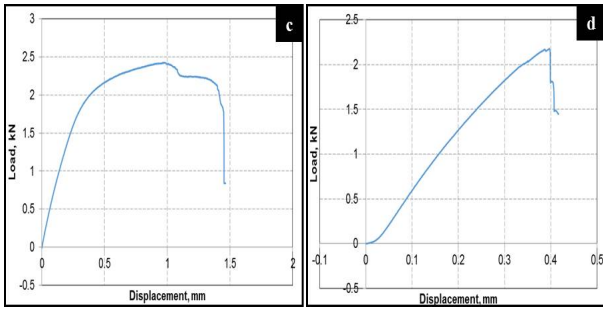
Figure 5. Load-displacement curves for Cu-Al-Mn SMA's.

3.2 Tensile properties

To understand the effect of Mn on the tensile behavior of Cu-Al-Mn SMA's, the yield strength, yield strain, and ultimate tensile strength were evaluated from the tension test. Fig. 5 shows the load-displacement curves for Cu-Al-Mn SMAs, and the tensile properties obtained from these curves are presented in Table 4. As seen in the figure, the SMA's C2 and C3 showed the β phase undergoing uniform elastic deformation with the stress increasing under varying ranges of strain. On the other hand, the SMA's C1, C4, and C3, up to some extent, showed quite a change in the slope, implying the occurrence of stress-induced martensitic transformation. Post this transformation the slope of all these SMA's remains unchanged until the failure. From the values of yield and ultimate tensile strength, it is quite clear that they increase with Mn content until 6 wt% and decrease after that. The ultimate tensile strength was highest for C3 alloy while lowest for C4 alloy. The addition of Mn resulted in control in the grain size and an increase in the number of grain boundaries [23]. So, the strengthening of material based on the size of the grains can be explained by the Hall-Petch relationship which proposes that strength is inversely proportional to the grain size. The higher the number of grain boundaries, the greater the difficulty of dislocation moving in the alloy, thereby enhancing its strength. In addition to inhibition to dislocation motion, the increase in grain boundary volume slows down the development of slips and reorientation of martensite variants which is quite evident from the higher slope in the load-displacement curve for all Cu-Al-Mn SMA's.

Table 4. Mechanical properties of Cu-Al-Mn SMA's

Sample ID	Ultimate tensile strength (MPa)	Yield strength (0.2%) (MPa)	Yield strain (0.2%)	Strain recovery by SME (%)
C1	365.22	139.73	7.05	91
C2	387.12	116.57	5.91	98
C3	404.26	147.43	4.96	100
C4	362.82	170.88	6.71	92

This is observed in the C2 and C3, which displayed higher strength values, but a decrease in the strength of the C4 alloy could be due to the depletion of precipitates [24]. As already men–tioned, the Mn-added alloys display higher strength due to precipitation hardening as well, but at higher content and processing conditions, the amount of precipitates might have depleted, which

decreased the strength of C4. In addition to a decrease in the grain size and pre–cipitation hardening, the degree of order also plays an important role. The degree of order increases along with the increase in Mn content. The movement of dislo–cations in the ordered structure is inhibited due to the high lattice frictional force imposed by it [25,26].
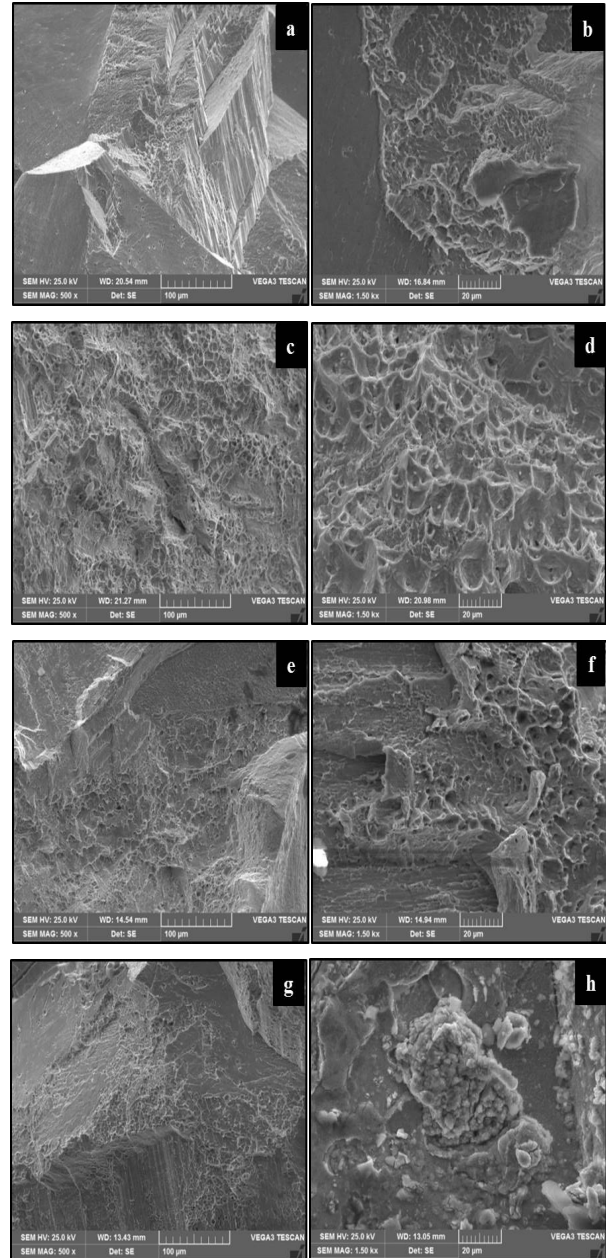

Figure 6. Tensile fracture surfaces of (a,b) C1, (c,d) C2, (e,f) C3 and (g,h) C4 SMA's

Many factors influence the initiation and propa–gation of the failure process in Cu-based SMA's, which include casting defects, anisotropy generated due to elastic and plastic incompatibilities in the micro–structure, segregation of impurities at the grain boun–daries, and stress-induced martensite [27,28]. Fig. 6 (a) – (d) shows the fracture surface of Cu-Al-Mn SMA's obtained after tensile test in low and high magnification micrographs. Despite the addition of a considerable amount of Mn to the Cu-Al alloy system, the fractured surface of all SMA's showed smooth cleavage surfaces (see Fig. 6 (a), (c), (e), and (g)). The macroscopically

seen smooth surface indicates brittle fracture, but microscopically, many regions showed fine dimples (see Fig. 6 (b), (d), (f), and (h)). The presence of dim–ples does suggest ductile failure, but based on the observations, it can be said that all alloys have under–gone mixed fracture mode [29].

3.3 Corrosion behavior

The corrosion behavior of Cu-Al-Mn SMA's in fresh water, substitute ocean water, and Hanks solutions were studied, and the results obtained in the form of poten–tiodynamic polarization curves are presented in Fig. 7 (a) – (l). The values of corrosion potential (E_{corr}) and corrosion current (i_{corr}) were extracted from the curves using the Tafel extrapolation methodology and provided in Table 5. The E_{corr} values for all cases of corrosive media were found to decrease with the increasing Mn content in the Cu-Al-Mn SMA's. When tested in fresh water, the E_{corr} values for C1 and C4 with the lowest and highest Mn content were -152.34 mV and -46.87 mV, respectively. Similarly, for the cases of substitute ocean water and Hank's solution, the highest value of E_{corr} was recorded for C1, while the lowest was recorded for C4. The trend indicates that addition and enhancement in Mn content in SMAs tend to reduce the corrosion reaction of alloy and shift the E_{corr} in a noble direction. Based on the potentials, Cu is most, and Al is least noble, implying the corrosion products formed on the surface are mainly composed of Al and Mn. A passive layer is formed due to a reaction between SMA's and corrosive media, which indicates its ability to protect naturally. Specifically, the passivation film formed due to electrochemical oxidation has Mn content, and in the case of SMA's with higher Mn content, the aggressive action of Cl^- is well resisted, thereby enhancing the corrosion resistance [19,30]. Based on the corrosion potentials, it can be said that despite being less noble than Cu, Mn is more capable of providing corrosion resistance against Cl^-. Overall, based on the higher negative E_{corr} values, it can be said that the addition of Mn can help in providing resistance, but the formed passive film is unstable and allows Cu to dissolve.
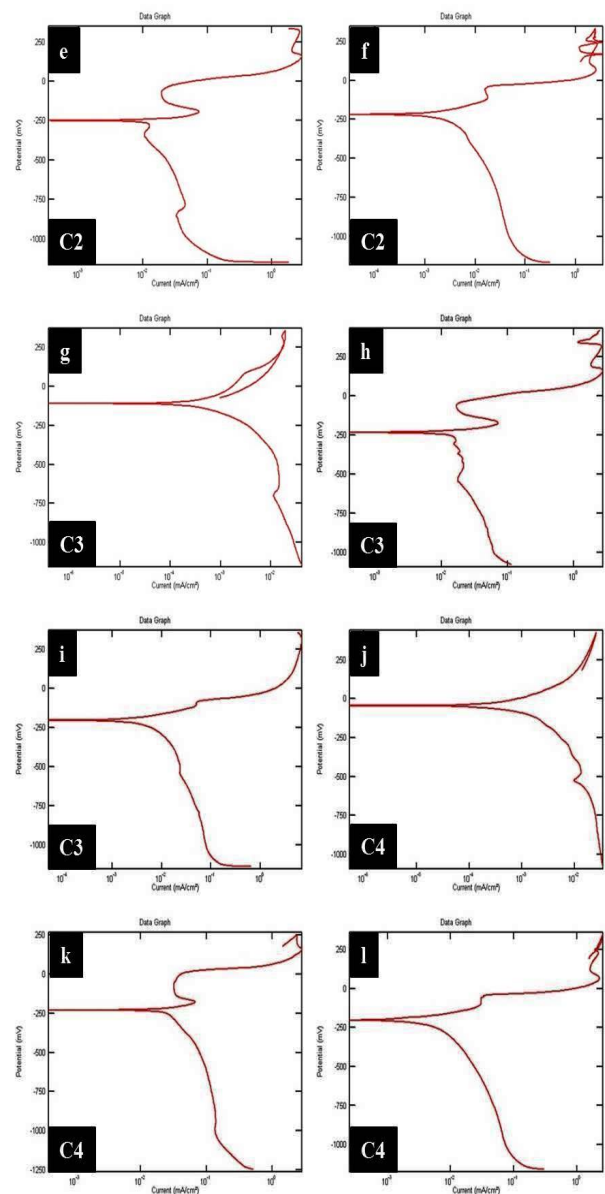

Figure 7. Potentiodynamic polarization curves for Cu-Al-Mn SMA's tested in (a,d,g,j) fresh water, (b, e, h, k) ocean water, and (c, f, i, l) Hank's solution.
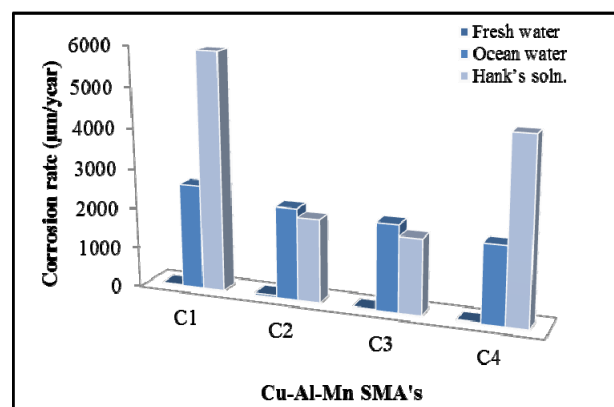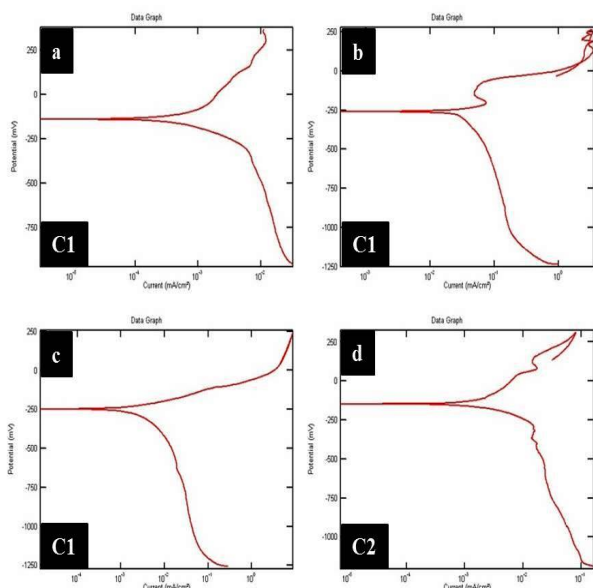

Figure 8. The corrosion rate of Cu-Al-Mn SMA's.

From i_{corr} point of view, the trend is not definite when compared to that of corrosion potential. For fresh–water, all trends are not clear as it tends to fluctuate and substitute ocean water, and Hank's solution showed a decreasing trend with Mn content.

Table 5 Corrosion potential of Cu-Al-Mn SMA's in different solutions

Testing solution	C1		C2		C3		C4	
	E_{corr} (mV)	i_{corr} (mA/cm^2)	E_{corr} (mV)	i_{corr} (mA/cm^2)	E_{corr} (mV)	i_{corr} (mA/cm^2)	E_{corr} (mV)	i_{corr} (mA/cm^2)
Fresh water	-152.34	0.0007	-148.43	0.0023	-109.37	0.0009	-46.87	0.0011
Ocean water	-265.62	0.1139	-250.0	0.0998	-234.37	0.0942	-226.56	0.0843
Hank's soln.	-250.0	0.2582	-210.93	0.0902	-203.12	0.0818	-195.31	0.1972

The lowest i_{corr} value of 0.0007 mA/cm^2 was observed for C1 in freshwater media, 0.0843 mA/cm^2 for C4 in substitute ocean water and 0.0818 mA/cm^2 for C3 in Hank's solution. The lower i_{corr} values suggest better corrosion resistance than other SMA's [31]. On the other hand, C2 in fresh water and C1 in substitute ocean water and Hank's solution showed higher score values, indicating a higher disso–lution rate. Based on this, it can be suggested that SMAs with higher Mn content provide better corrosion resis–tance, except for the case of SMAs tested in fresh water. The corrosion rate was calculated using the following relationship [30],

$$Pi = 22.85\ i_{corr}$$

The calculated corrosion rate/year is presented in Fig. 8. Compared to substitute ocean water and Hank's solu–tion, the corrosion rate/year for SMA's tested in fresh–water is very minimal. Although there was no definite trend but the highest corrosion rate of 52.56 μm/year was observed for C2 SMA. In the case of substitute ocean water and Hank's solution the highest corrosion water of 2602.62 μm/year and 5899.87 μm/year was observed for C1 SMA. However, the overall trend suggests a decrease in corrosion rate with an increase in Mn content.

Post-corrosion tests in different corrosion media, the SMAs were examined using SEM and presented in Fig. 9 (a)–(f). In the case of C1 and C3 SMA's tested in fre–sh water, the corroded surface showed a thin and porous passivation film (Fig. 9 (a) and (b)). Several regions had a high accumulation of corrosion products. Based on the corrosive media, the products formed are cuprous oxide or aluminum hydroxide. Further, it can be said that the selective dissolution of Al and Mn indicates pitting corrosion in these SMAs. In the case of SMAs tested in substitute ocean water, the corroded surfaces of C1 and C3 were covered with cracked corrosion pro–ducts (Fig. 9 (c) and (d)). The thickness of corrosion products can be observed via the depth of cracks that penetrated to larger depths. However, the C3 SMA, which had higher Mn content, significantly decreased the thickness and amount of corrosion products. So, it can be said that the formation of corrosion products varies based on the Mn content in the SMA's. Similar features were seen for C1 and C3 SMAs tested in Hank's solution, but the accu–mulation of corrosion products was high in some regi–ons (see Fig. 9 (e) and (f)). The EDAX analysis was conducted on C1 SMA and tested in substitute ocean water and Hank's solution to understand the compo–sition of the corrosion products accumulated on the cor–roded surface. The elements pre–sent in the corrosion products seen on C1 SMA tested in substitute ocean water were Al, Cu, Mn, Cl, and O ((see Fig. 10 (a)). The presence of high-intensity peaks of Al, Cl, and O suggests the formation of aluminum oxide, which indicates

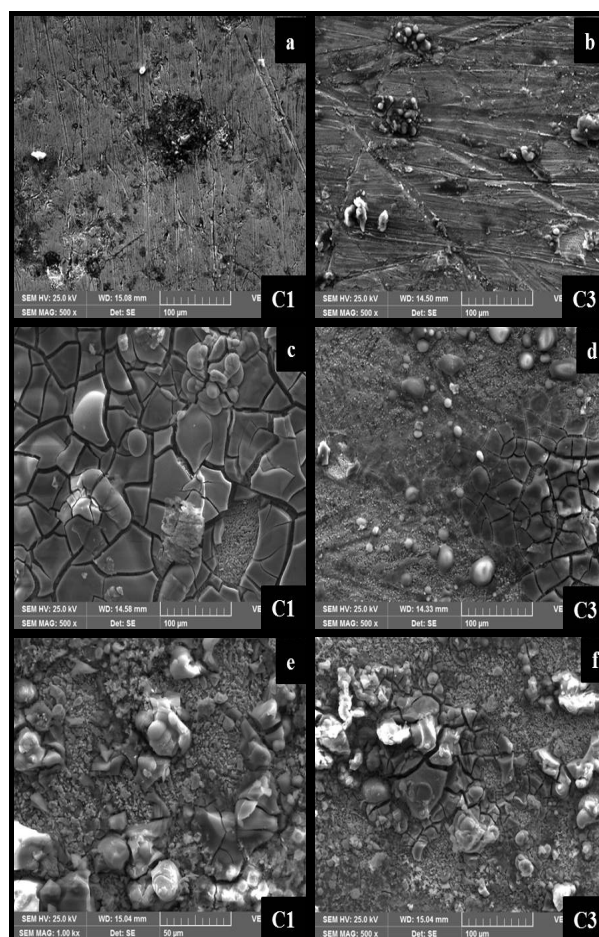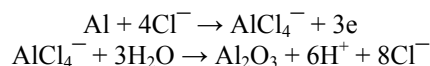the dissolution of Al. The formation of aluminum oxide can be understood via the following reactions [32],

$$Al + 4Cl^- \rightarrow AlCl_4^- + 3e$$
$$AlCl_4^- + 3H_2O \rightarrow Al_2O_3 + 6H^+ + 8Cl^-$$

Figure 9. SEM micrographs of Cu-Al-Mn SMAs were tested in (a,b) fresh water, (c,d) substitute ocean and (e,f) Hank's solution.

Similarly, the Mn hydroxide and oxide are also for–med on the corroded surface which can be understood via the following reactions.

$$Mn^{2+} + 2H_2O \rightarrow Mn(OH)_2 + 2H^+$$
$$2\ Mn(OH)_2 + O_2 \rightarrow 2MnO_2 + 2H_2O$$
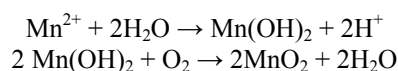
The lower amount of Cu seen in the EDAX profile suggests a thick layer of Al and Mn-based oxides on the surface. Although the formation of Cu_2O, Al_2O_3, and MnO_2 provides corrosion resistance to the SMA, it is unstable, which is why the accumulation of corrosion products is larger in several regions. The removal of the corrosion layer and damaged SMA surface underneath indicates the intensity of corrosive media and the pas-sivation of instability despite the formation of oxides mentioned above or hydroxides. Further, Fig. 10 (b)

shows the EDAX profile of C1 SMA tested in Hank's solution, which had almost all elements that were seen in the previous case except for the fact that Cu, Al, and Cl showed high-intensity peaks. Since this SMA showed a high corrosion rate, the dissolution of Cu and Al can be understood well based on their high-intensity peaks.
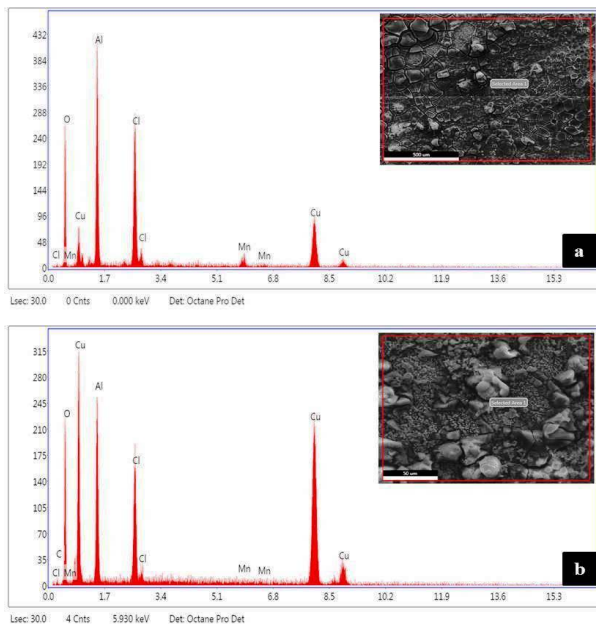

Figure 10. EDAX analysis of C1 in (a) substitute ocean water and (b) Hank's solution post-corrosion testing.

4. CONCLUSION

In this work, an attempt was made to understand the effect of varying Mn on the mechanical and corrosion behaviour of Cu-Al-Mn SMA's.

➢ About 6 wt% Mn content facilitated Cu-Al-Mn SMA alloy to attain strain recovery of 100% by SME.

➢ Both yield and ultimate tensile strength of Cu-Al-Mn SMA's tend to increase up to 6 wt% Mn content and tend to decrease after that. The strengthening of the alloys was attributed to grain refinement and precipitation hardening.

➢ The tensile fractured surfaces provided insight on fracture mode of Cu-Al-Mn SMA's. All of them showed mixed mode failure as they displayed both cleavage and dimples on the fracture surface.

➢ The addition of mn to Cu-Al-Mn SMA's decreased the corrosion potential, corrosion current density, and corrosion rate. This behaviour is quite evident when tested in substitute ocean water and Hank's solution.

➢ The corroded surface analysis of SMA with low Mn content showed a weak and unstable surface layer. The cracked surface layer suggests the dissolution of alloy and low corrosion resistance. For fresh water tested SMA, the corroded surface displayed pitting corrosion.

Overall, the work showed that enhancement in Mn content up to 6 wt% is beneficial in enhancing strength and corrosion resistance of Cu-Al-Mn SMA's.

REFERENCES

[1] Chang, L.C. Read, T.A.: Plastic deformation and diffusionless phase changes in metals - the Gold-cadmium beta phase, JOM, Vol. 3, pp. 47-52, 1951.

[2] Tadaki, T., Otsuka, K. Shimizu, K.: Shape memory alloys, Annu. Rev. Mater. Sci., Vol. 18, pp. 25-45, 1988.

[3] Otsuka, K. Ren, X.: Recent developments in the re-search of shape memory alloys, Intermetallics, Vol. 7, pp. 511-528, 1999.

[4] Hart, D.J., Lagoudas, D.C.: Aerospace applications of shape memory alloys, Proc. Inst. Mech. Eng. G: J. Aerosp. Eng., Vol. 221, pp. 535-552, 2007.

[5] Petrini, L., Migliavacca, F.: Biomedical applicati-ons of shape memory alloys, J. Metall., Vol. 2011, Article ID 501483, 2011.

[6] Habu, T.: Applications of shape memory alloys (SMAs) in electrical appliances, in: Yamauchi, K., Ohkata, I., Tsuchiya, K. and Miyazaki, S. (Eds.): *Shape memory and superelastic alloys: Applica-tions and technologies*, Woodhead Publishing Limited, pp. 87-99, 2011.

[7] Zareie, S. Issa, A.S., Seethaler, R.J. Zabihollah, A.: Recent advances in the applications of shape memory alloys in civil infrastructures: A review, Structures, Vol. 27, pp. 1535-1550, 2020.

[8] Shape memory alloys market, Market research rep-ort, Report code CH 6263, published on July 2021.

[9] Dasgupta, R.: A look into Cu-based shape memory alloys: Present scenario and future prospects, J. Mater. Res., Vol. 29, pp. 1681-1698, 2014.

[10] Kainuma, R., Takahashi, S., Ishida, K.: Thermo-elastic martensite and shape memory effect in ductile Cu-Al-Mn alloys, Metall. Mater. Trans. A, Vol. 27, pp. 2187-2195, 1996.

[11] Mallik, U.S., Sampath, V.: Influence of quaternary alloying additions on transformation temperatures and shape memory properties of Cu-Al-Mn shape memory alloy, J. Alloys Compd., Vol. 469, pp. 156-163, 2009.

[12] Raju, T.N., Sampath, V.: Effect of ternary addition of iron on shape memory characteristics of Cu-Al alloys, J. Mater. Eng. Perform., Vol. 20, pp. 767-770, 2011.

[13] Pinto, R.D.A., Ferreira, L.D.R., Silva, R.A.G.: Size matters: Influence of atomic radius from the ternary addition on the properties of $Cu_{79}Al_{19}X_2$ (X = Be, Mn, Ag) alloys, Mater. Chem. Phys., Vol. 294, pp. 127021, 2023.

[14] Moskvichev, E., Shamarin, N., Smolin, A.: Structure and mechanical properties of Cu-Al-Mn Alloys fabricated by electron beam additive manufacturing, Materials, Vol. 16, pp. 123, 2023.

[15] Benedeti, A.V., Sumodjo, P.T.A., Nobe, K., Cabot, P.L., Proud, W.G.: Electrochemical studies of copper, copper-aluminium and copper-aluminium-silver alloys: Impedance results in 0.5M NaCl, Electrochim. Acta, Vol. 40, pp. 2657-2668, 1995.

[16] Ashour, E.A., Ateya, B.G.: Electrochemical behaviour of a copper-aluminium alloy in concentrated al-

kaline solutions, Electrochim. Acta, Vol. 42, pp. 243-250, 1997.

[17] Montecinos, S., Simison, S.: Corrosion behavior of Cu-Al-Be shape memory alloys with different compositions and microstructures, Corros. Sci., Vol. 74, pp. 387-395, 2013.

[18] Vrsalovic, L., Ivanic, I., Kozuh, S., Gudic, S., Kosec, B., Gojic, M.: Effect of heat treatment on corrosion properties of CuAlNi shape memory alloy, Trans. Nonferrous Met. Soc. China, Vol. 28, pp. 1149-1156, 2018.

[19] Vrsalovic, L., Ivanic, I., Kozuh, S., Kosec, B., Bizjak, M., Kovac, J., Gabor, U., Gojic, M.: Influence of heat treatment on the corrosion pro–perties of CuAlMn shape memory alloys, Corros. Rev., Vol. 37, pp. 579-589, 2019.

[20] Shivasiddaramiah, A.G., Mallik, U.S., Mahato, R., Shashishekar, C.: Evaluation of corrosion behaviour of Cu-Al-Be-Mn quaternary shape memory alloys, Mater. Today Proc. Vol. 4, pp. 10971-10977, 2017.

[21] Saud, S.N., Hamzah, E., Abubakar, T., Ibrahim, M.K., Bahador, A.: Effect of a fourth alloying element on the microstructure and mechanical properties of Cu-Al-Ni shape memory alloys, J. Mater. Res., Vol. 30, pp. 2258-2269, 2015.

[22] Guo, L. et al.: The improvement of the shape memory effect of Cu-13.5Ale4Ni high temperature shape memory alloys through Cr-, Mo, or V-alloying, J. Sci.: Adv. Mater. Devices, Vol. 8, pp. 100532, 2023.

[23] Mazzer, E.M., da Silva, M.R., Gargarella, P.: Revisiting Cu-based shape memory alloys: Recent developments and new perspectives, J. Mater. Res., Vol. 37, pp. 162-182, 2022.

[24] Zhang, G., Yin, H., Zhang, C., Deng, Z., Zhang, R., Jiang, X., Qu, X.: Effect of Mn on microstructure and properties of Cu-12Al powder metallurgy alloy, Mater. Res. Express, Vol. 7, pp. 016546, 2020.

[25] Koti, V., George, R., Shakiba, A., Murthy, K.V.S.: Mechanical properties of copper nanocomposites reinforced with uncoated and nickel coated carbon nanotubes, FME Trans., Vol. 46, pp. 623-630, 2018.

[26] Mallikarjuna, H.M., Siddaraju, C., Kumar, H.S.S., Koppad, P.G.: Nanohardness and wear behavior of copper-SiC-CNTs nanocomposites, FME Trans., Vol. 48, pp. 688-692, 2020.

[27] Krstic, B., Rasuo, B., Trifkovic, D., Radisavljevic, I., Rajic, Z., Dinulovic, M.: Failure analysis of an aircraft engine cylinder head, Eng. Fail. Anal., Vol. 32, pp. 1-15, 2013.

[28] Krstic, B., Rasuo, B., Trifkovic, D., Radisavljevic, I., Rajic, Z., Dinulovic, M.: An investigation of the repetitive failure in an aircraft engine cylinder head, Eng. Fail. Anal., Vol. 34, pp. 335-349, 2013.

[29] Yang, L., Jiang, X., Sun, H., Shao, Z., Fang, Y., Shu, R.: Effects of alloying, heat treatment and nano reinforcement on mechanical properties and damping performances of Cu-Al-based alloys: A review, Nanotechnol. Rev., Vol. 10, pp. 1560-1591, 2021.

[30] Saud, S.N., Hamzah, E., Abubakar, T., Bakhsheshi-Rad, H.R., Zamri, M., Tanemura, M.: Effects of Mn additions on the structure, mechanical properties, and corrosion behavior of Cu-Al-Ni shape memory alloys, J. Mater. Eng. Perform., Vol. 23, pp. 3620-3629, 2014.

[31] Gudic, S., Rakuljic, B., Vrsalovic, L., Bizjak, M., Ivanic, I., Kozuh, S., Gojic, M.: Influence of Mn on the corrosion behavior of CuAlMn alloy in NaCl solution, in: 18th International Foundrymen Con–ference, Coexistence of material science and sustai–nable technology in economic growth, May 15th – 17th, 2019, Sisak.

[32] Saud, S.N., Hamzah, E., Abubakar, T., Bakhsheshi-Rad, H.R.: Correlation of microstructural and corros–ion characteristics of quaternary shape memory alloys Cu-Al-Ni-X (X=Mn or Ti), Trans. Nonferrous Met. Soc. China, Vol. 25, pp. 1158-1170, 2015.

NOMENCLATURE

θ_m	Angle recovered after unloading
θ_e	Angle recovered after heating
E_{corr}	Corrosion potential
i_{corr}	Corrosion current
P_i	Corrosion rate

УТИЦАЈ ВАРИЈАЦИЈА У САДРЖАЈУ МН НА МЕХАНИЧКЕ И КОРОЗИОНЕ КАРАКТЕРИСТИКЕ Cu-Al-Mn ЛЕГУРА СА МЕМОРИЈОМ ОБЛИКА

К.М. Маматха, У.С. Малик, В. Коти, К.В.Ш. Мурти, П.Г. Копад

У овом раду проучавана је улога Мн на ефекат меморије облика и механичко и корозионо пона–шање легура са меморијом облика Cu-Al-Mn. Сас–тав Al је фиксиран на 10 теж%, док је Mn варирао од 2 до 10 теж.%. Опоравак од деформације код СМЕ је процењен тестом савијања, док су попуштање и гранична затезна чврстоћа добијени тестом зате–зања. Понашање корозије је проучавано кориш–ћењем три различита раствора: слатке воде, замен–ске океанске воде и Хенковог раствора. Принос и гранична затезна чврстоћа легура Cu-Al-Mn пове–ћани су са садржајем Mn до 6%, што се приписује пречишћавању зрна и таложном очвршћавању, док је анализа лома показала мешовити режим неуспеха за све легуре. Корозивно понашање легура Cu-Al-Mn је модификовано због додавања Mn. Са пове–ћањем садржаја Mn, легуре су показале бољу отпо–рност на корозију и ниже стопе корозије. Анализа кородиране површине која је тестирана у слаткој води показала је питинг корозију, док је легура Cu-Al-Mn са ниским садржајем Mn тестирана у замени океанске воде. Хенково решење показало је повр–шинско оштећење са нестабилним површинским слојем.